Materials Science in Semiconductor Processing 67 (2017) 75–83

Contents lists available at ScienceDirect

Materials Science in Semiconductor Processing

journal homepage: www.elsevier.com/locate/mssp

Comparative study between CBD and SILAR methods for deposited TiO_2, CdS, and TiO_2/CdS core-shell structure

Selma M.H. Al-Jawad

Applied Science Department, University of Technology, Baghdad, Iraq

ARTICLE INFO

Keywords:
TiO_2/CdS core–shell
CBD
SILAR
PEC performance

ABSTRACT

TiO_2, CdS, and TiO_2/CdS core–shell structures were deposited on fluorine-doped tin oxide (FTO)-coated glass substrate using chemical methods. TiO_2 thin films were prepared by chemical bath deposition (CBD) and successive ionic layer adsorption and reaction (SILAR). SILAR was also utilized to deposit CdS film on TiO_2 thin film. The structural, surface morphology, and optical characteristics of FTO/TiO_2, FTO/CdS, and FTO/TiO_2/CdS core- shell structures were evaluated. The FTO/TiO_2 films produced by both methods conformed to anatase and rutile phase structures. Corresponding XRD pattern of the FTO/TiO_2/CdS sample exhibited one peak corresponding to hexagonal (101) for CdS. Scanning electron micrographs showed nanorod structures for the TiO_2 thin films deposited by CBD, contrary to the nanograin structure formed by SILAR. Optical results showed highly extended absorption edge to the visible region for the FTO/TiO_2/CdS structure deposited by the two methods. The TiO_2 thin films deposited by CBD exhibited higher absorption in the visible region than nanograined TiO_2 thin films deposited by SILAR because of the high surface area of the TiO_2 nanorod. Photoelectrochemical (PEC) properties of FTO/TiO_2, and FTO/TiO_2/CdS system were also examined. PEC behavior of FTO/TiO_2/CdS was compared with that of FTO/TiO_2 deposited by CBD and SILAR. The TiO_2 nanorod thin films deposited by CBD showed evidently enhanced PEC performance compared with nanograined TiO_2 thin films deposited by SILAR.

1. Introduction

Core–shell oxide materials are rarely investigated. However, production of metal particles with core–shell structures has been attracting attention because of their vast applications in technological fields. A core–shell thin film consists of a core and a coating shell made of different materials. Easy variation of the core and shell structures leads to innovations because of the useful properties of these structures in various fields such as cellular imaging sensors, coating, biosensor, and magnetic orientation of animals [1].

TiO_2 has n-type conductivity because of oxygen vacancies in its structure. The conductivity of TiO_2 increases with the degree of oxygen loss in the lattice. TiO_2 thin film is one of the most investigated transparent conductive oxides because of its attractive physical, chemical, and optoelectronic properties [2]. This thin film exhibits good transmittance in the visible region, high refractive index, high dielectric constant, high photocatalytic activity, and chemical stability. Furthermore, the surface of TiO_2 exhibits high hydrophilicity under UV light irradiation [3,4].

Numerous studies on the preparation of nanostructured TiO_2 have focused on controlling the morphology and particle size. These nanostructures have been deposited using several methods, such as chemical bath deposition (CBD) [1], successive ionic layer adsorption and reaction (SILAR) [5,6], anodic oxidation [7], sol–gel [8–10], spray pyrolysis [11–13], DC magnetron sputtering [14], liquid phase deposition technique [15], and hydrothermal process [16]. SILAR and CBD methods are inexpensive and performed at low temperature. These processes produce nanostructured thin films with large surface area [5,17–19].

One important approach is to prepare TiO_2 using different materials, such as metallic nanoparticles (NPs) and dyes as sensitizers, which enhance the photo-activity of TiO_2 in the visible region of the spectrum. Mixing two semiconductor particles facilitates the preparation of a semiconductor material with large energy gap and energetically low-lying conduction band by another one with small energy gap and energetically high-lying conduction band. An efficient and longer charge separation can be achieved by injecting a charge from one semiconductor into another. This process presents potential applications in photocatalysis and solar cell. In particular, cadmium chalcogenide nanocrystalines are very attractive as sensitizers for TiO_2 because of their size-tunable optical properties. Principally, CdS is a photoconducting and active sensitizer material, because its energy band

E-mail address: 100069@uotechnology.edu.iq.

http://dx.doi.org/10.1016/j.mssp.2017.05.014
Received 12 February 2017; Received in revised form 1 May 2017; Accepted 9 May 2017

coincides with the energy of TiO_2 [6].

Challa et al. [20] fabricated TiO_2/CdS core–shell nanowires (NWs) via a two-step process. First, the TiO_2 nanowires were synthesized using a simple thermal oxidation treatment of a Ti film, followed by O_2 plasma treatment. CdS was then coated by low-cost CBD. The TiO_2/CdS core-shell nanowires showed much longer photoluminescence (PL) lifetimes than the CdS film because of the electron–hole separation across the TiO_2 and CdS interface. Deshmukh et al. [6] investigated the surface morphology, structure, and optical and photoelectrochemical (PEC) behavior of FTO/TiO_2/CdS bilayers and compared these bilayers with FTO/CdS singular structure. FTO/TiO_2, FTO/CdS, and FTO/TiO_2/CdS photo-electrodes were synthesized successfully by employing low-temperature chemical means on the fluorine-doped tin oxide-coated glass substrate (FTOCGS). TiO_2 was deposited on FTOCGS by SILAR. CBD was used to deposit CdS thin films on previously prepared TiO_2 film. Cao et al. [21] enhanced the PEC performance of the TiO_2/CdS core–shell heterojunction. This heterojunction consisted of vertically aligned TiO_2 nanorod (NR) prepared by a surface hydrothermal process and CdS NPs deposited on TiO_2 NRs by spin-coating–SILAR. Hu et al. [22] prepared TiO_2 NRs using hydrothermal technique without a seed layer and CdS quantum dots (QDs) by SILAR followed by thermal annealing. Xie et al. [23] sensitized TiO_2 NR arrays (NRAs) with CdS NPs manufactured by SILAR, and TiO_2 NRAs were obtained by oxidizing Ti NRAs produced from oblique angle deposition. TiO_2 NRA/CdS NP composites provide a promising way of manufacturing material for solar cell and wastewater purification. Li et al. [24] employed a simple hydrothermal treatment to directly grow TiO_2 nanowire (NW) membranes on Ti substrates followed by annealing and sensitizing TiO_2 NWs with CdS QDs using CBD. Yu et al. [25] fabricated CdS NPs decorated anatase TiO_2 nanotubes through an alkaline hydrothermal method combined with surface precipitation technique. CdS NPs were deposited onto the surfaces of titanium nanotubes by reacting Na_2S with Cd^{2+} ions. Numerous studies have reported the fabrication of TiO_2/CdS core–shell system. However, review of literature shows the absence of report on the characterization of thin films to define the structure, surface morphology, and optical properties of materials using CBD and SILAR, because SILAR is a new and less investigated technique. In this study, TiO_2 film was deposited on FTOCGS using CBD and SILAR, and the resulting films were compared. SILAR was utilized for CdS thin-film deposition on pre-deposited TiO_2 film. Then, the structure, morphology, and optical characteristics of FTO/TiO_2 and FTO/TiO_2/CdS core–shell system were investigated. The PEC behavior of FTO/TiO_2/CdS was also studied and compared with FTO/TiO_2 deposited by the two methods.

2. Experimental work

2.1. TiO_2 thin film deposited by CBD

The FTO glass substrates were cleaned by detergent and deionized water to pretreat the substrate surfaces. Then, the substrates were cleaned using ammonia and finally rinsed by acetone. CBD was employed because of its suitability in depositing films on a substrate with large area and cost-effectiveness [1]. The core of the TiO_2 films was prepared from 0.8 mL of 1 M of $TiCl_3$, 0.3 mL of 1 M of NaOH, and 0.35 mL of polyvinyl alcohol (PVA) at 80 °C bath temperature and 3 h of deposition time. The sample was prepared at pH 2.

2.2. TiO_2 thin film deposited by SILAR

TiO_2 thin film was grown at room temperature by SILAR. The positive ion was provided by the aqueous solution of 0.1 M $TiCl_3$, 30% HCl, and 0.01 M NaOH. The FTOCGS was immersed for 20 s in a cationic precursor, during which the absorption of complex titanium species occurred. The FTOCGS was rinsed for 5 s by doubled-distilled water and then immersed for 20 s in an anionic precursor, where NaOH reacted with Ti to form TiO_2 on the FTOCGS. The unreacted species or deposited powders were removed from the FTOCGS by again rinsing the substrate for 5 s. Finally, the samples were treated thermally for 2 h at 400 °C to remove hydroxide and improve crystallinity.

2.3. Synthesis and deposition of CdS by SILAR

CdS QDs were deposited on the TiO_2 thin films using SILAR technique. A substrate made of FTO material was grown with TiO_2 films and immersed for 2 min in an aqueous solution of 0.3 mol/L Cd $(CH_3COO)_2$, rinsed with deionized water, immersed in a 0.3 mol/L Na_2S aqueous solution and again for 2 min, and finally washed with deionized water. These steps were performed to synthesize the CdS QDs and were repeated several times until a thin QD layer was formed.

The structures of TiO_2 and CdS QDs were investigated using X-ray diffraction (XRD) with CuKα radiation (k = 0.154 nm) in the 2θ range of 20–60°. The optical transmittance of the deposited thin film on FTO substrate was measured using UV–visible spectrophotometer (Metratech) in the wavelength range of 320–700 nm. Films thickness was measured by TF Probe ™ Spectroscopy-Angstrom Sun Tech. Inc. – USA/model SR 300-2012. The absorption coefficient and energy gap of films were evaluated using the optical transmittance spectra. Photoluminescence (PL) spectra were recorded by VARIAN/CARY Eclipse Fluorescence spectrophotometer with Xe flash lamp source (with excitation intensity at 300 nm from a Xe flash lamp as the excitation source).

The morphologies of the resulting films were characterized by atomic force microscopy (AFM; CSPM-500 Csp M-5000, USA-20080) and scanning electron microscopy (SEM; VEGA TESCAN) with energy dispersive X-ray (EDX) spectrometer, which provides the atomic qualitative and quantitative information from the specimen.

Photocurrent intensity with potential measurements was analyzed in the electrolyte solution of $NaNO_3$ (0.1 M). A three-electrode system was used. This system included TiO_2 and TiO_2/CdS as working electrode, a Pt foil as counter electrode, and a KCl-saturated Ag/AgCl as reference electrode. The illumination source was AM1.5G light at 100 mW/cm^2. The working electrode was illuminated with a 300 W Xe lamp.

3. Results and discussion

3.1. Structural study

Fig. 1 displays the XRD patterns of FTO and FTO/TiO_2 deposited by CBD. The films were polycrystalline with tetragonal structure mixed with anatase and rutile forms. The detected peaks were at 25.15°,

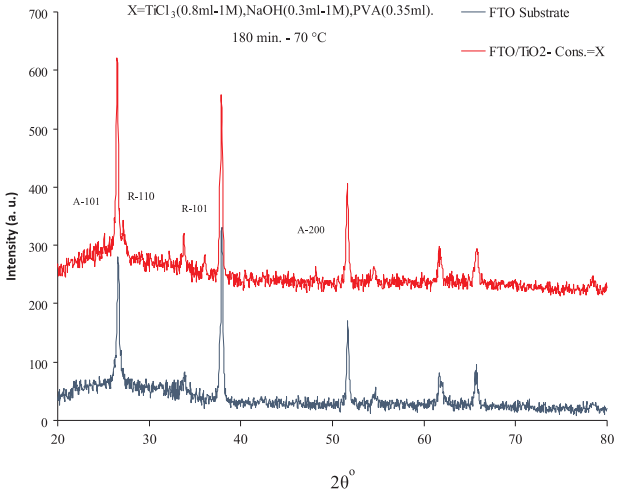

Fig. 1. XRD for TiO_2 thin film deposited by CBD.

Table 1
Crystallite size of the TiO_2 films.

Chemical method	CBD	SILAR (one cycle)	SILAR (five cycles)	SILAR (10 cycles)
Crystallite size (nm)	8	5	12	15

27.23°, 36.18°, and 48.2°, corresponding to the lattice planes A(101), R (110), R(101), and A(200). These results are in good agreement with the standard JCPD Nos. 21-1272 and JCPD No. 21-1276. The broad peak that appeared in the diffraction patterns indicates the small crystallite size and crystalline nature of the NRs [23]. The TiO_2 NRs were polycrystalline and consisted of anatase and rutile phases. The anatase–rutile heterojunction in the NRs may help the rutile particles to efficiently collect photon-induced electrons from the anatase particles to reduce charge recombination [26].

The crystallite size is estimated using Scherer's equation using the full width at half maximum (FWHM) of the (101) diffraction peak of anatase TiO_2 [27,28], as follows:

$$D = k\,\lambda/\beta cos\,\theta \quad (1)$$

where λ is the wavelength of the incident radiation in nanometers, D is the crystallite size in nanometers, $k = 0.90$ which is a constant, β is the FWHM in radians, and θ is Bragg's angle. The estimated crystallite sizes of the thin films are listed in Table 1.

Fig. 2 illustrates the XRD patterns of FTO and FTO/TiO_2 for one cycle and FTO/TiO_2 for five and ten cycles deposited by SILAR. The films exhibited anatase and rutile phases. The diffraction peak at $2\theta = 27.35°$ corresponding to the (110) crystal planes of the rutile phase is observed in addition to (101) crystal plane. XRD detected only (101) with anatase phase, and the intensity of the peak increased with the number of cycles. The weak intensity and broadness of diffraction peaks suggest the presence of some amorphous phase. These results are in agreement with that of previous studies [6].

The estimated crystallite sizes of the films are listed in Table 1.

Fig. 3 demonstrates the XRD patterns of FTO and TiO_2 deposited by CBD and TiO_2 with CdS NPs deposited by SILAR. The more predominant background peaks of FTO hampered the analysis. Thus, the importance of the structural study of FTO/TiO_2/CdS XRD pattern was reduced. All diffraction peaks for FTO/TiO_2/CdS at $2\theta = 25.2°$/A(101), 27.5°/R(110),and 36.2°/R(101) could be well indexed by the tetragonal anatase and rutile phases of TiO_2 (JCPDS No. 21-1272 and 21-1276). The structure of the TiO_2 deposited with CdS NPs was illustrated by measuring the sample by XRD with step scanning technique at scanning rate of 0.05°/step in the 25–28.5° scanning range. The resulting diffraction pattern of the FTO/TiO_2/CdS film is depicted in the inset of Fig. 3. The results show one peak at 28.2°, corresponding to

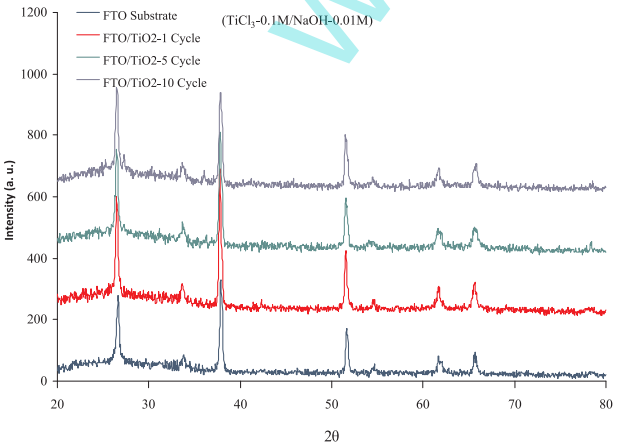

Fig. 2. XRD for TiO_2 thin film deposited by SILAR for different cycles.

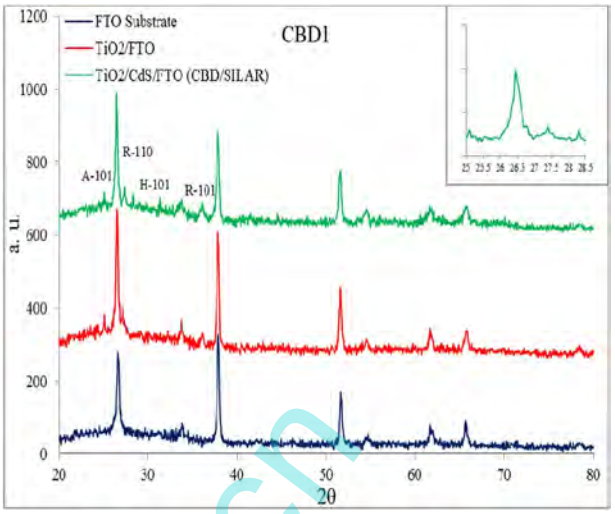

Fig. 3. XRD for FTO/TiO_2/CdS thin films (TiO_2-CBD/CdS-SILAR). Inset is the XRD pattern of TiO_2/CdS by step scanning method in the scanning range of 25–28.5°.

hexagonal (101) for CdS (JPCDS No. 41-1049) with two additional distinctive peaks for TiO_2, that is, one peak at 25.2° corresponding to anatase (101) and the other peak at 27.5° corresponding to rutile (110). The broader peak of the FTO is attributed to the amorphous/poorly crystalline TiO_2/CdS bilayers. Chen et al. [29] and Deshmukh et al. [6] reported similar amorphous nature of CdS over TiO_2 nanotube and NRs, respectively.

Fig. 4 exhibits the XRD patterns of FTO and FTO/TiO_2 deposited by SILAR and TiO_2 with CdS NPs deposited by SILAR. The XRD pattern of FTO/TiO_2/CdS shows the TiO_2 film deposited by SILAR on FTO substrates peaks on $2\theta = 25.3°$, 27.55°, and 36° corresponding to A(101), R(110), and R(101) crystalline planes of the anatase and rutile-tetragonal phases (JCPDS No. 21-1272 and 21-1276). Fig. 4 shows that a very weak peak reappeared to CdS deposited on TiO_2 film by SILAR method for one cycle with $2\theta = 28.08°$/(101) crystalline planes of hexagonal phase (JCPDS No. 41-1049). SILAR allows the formation of amorphous/poorly crystalline TiO_2/CdS bilayers system over the FTO substrate. These results are in agreement with previous published results [6].

3.2. Morphological study

The scanning electron micrographs of TiO_2 thin films deposited by CBD on FTOCGS are displayed in Fig. 5. The films were homogeneous and approximately uniformly deposited over the substrate surface. The

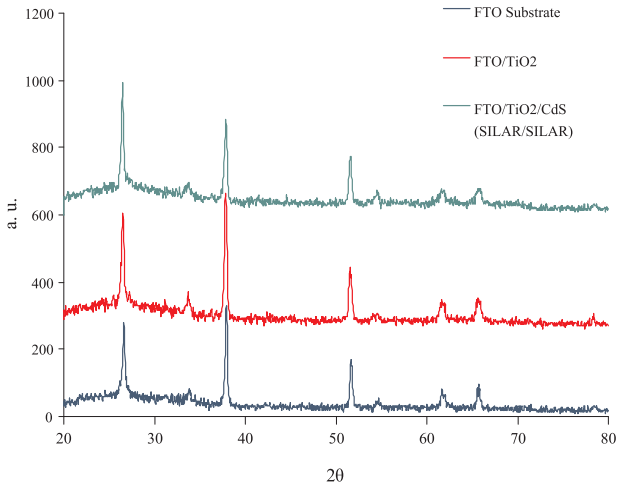

Fig. 4. XRD for FTO/TiO_2/CdS thin films (TiO_2- SILAR/CdS-SILAR).

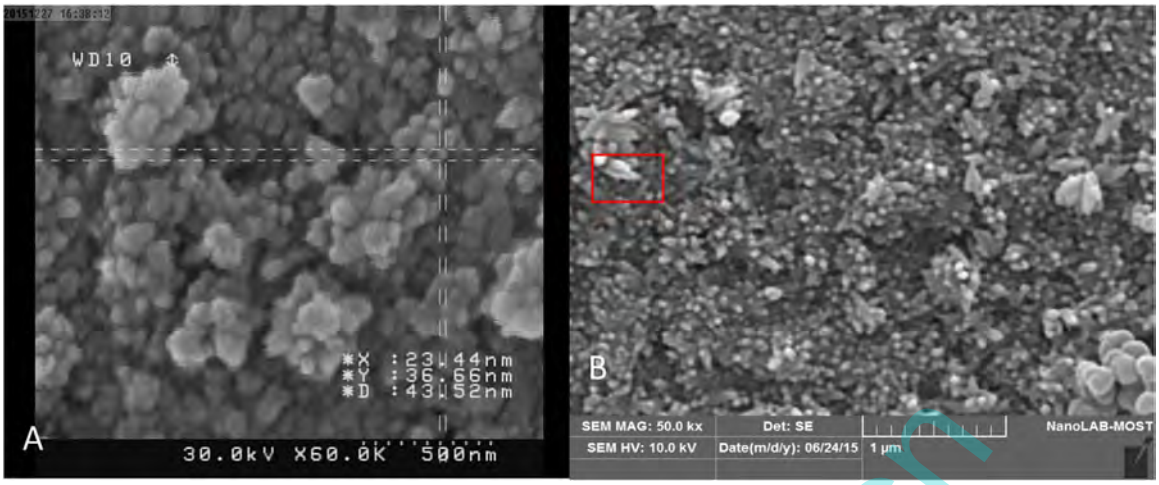

Fig. 5. SEM micrographs of FTO/TiO_2 deposited by CBD (A) with high magnification. (B) with low magnification (red square shows nanorods). (For interpretation of the references to color in this figure legend, the reader is referred to the web version of this article).

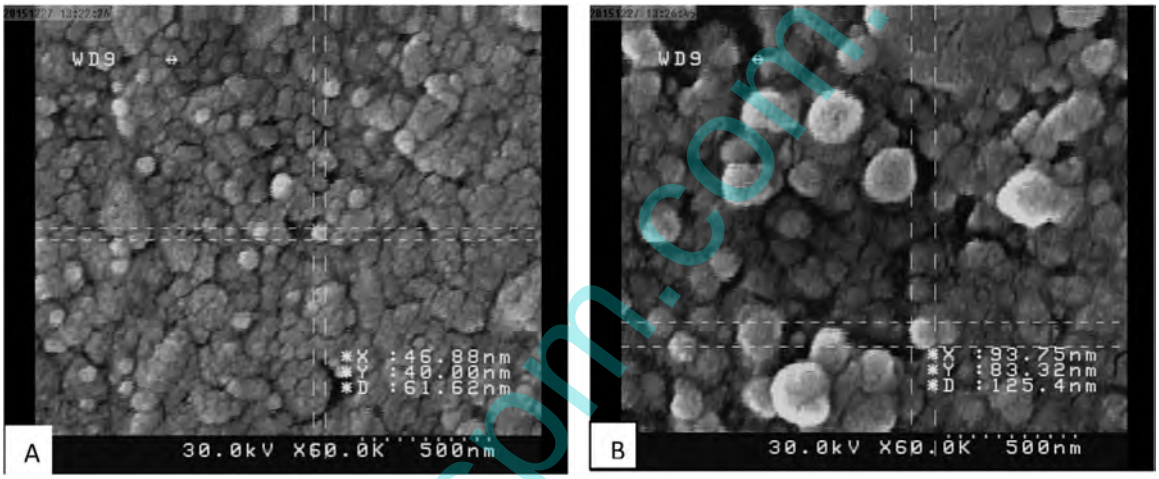

Fig. 6. SEM micrographs of (A) FTO/TiO_2 deposited by SILR for one cycle. (B) FTO/TiO_2 deposited by SILAR for ten cycles.

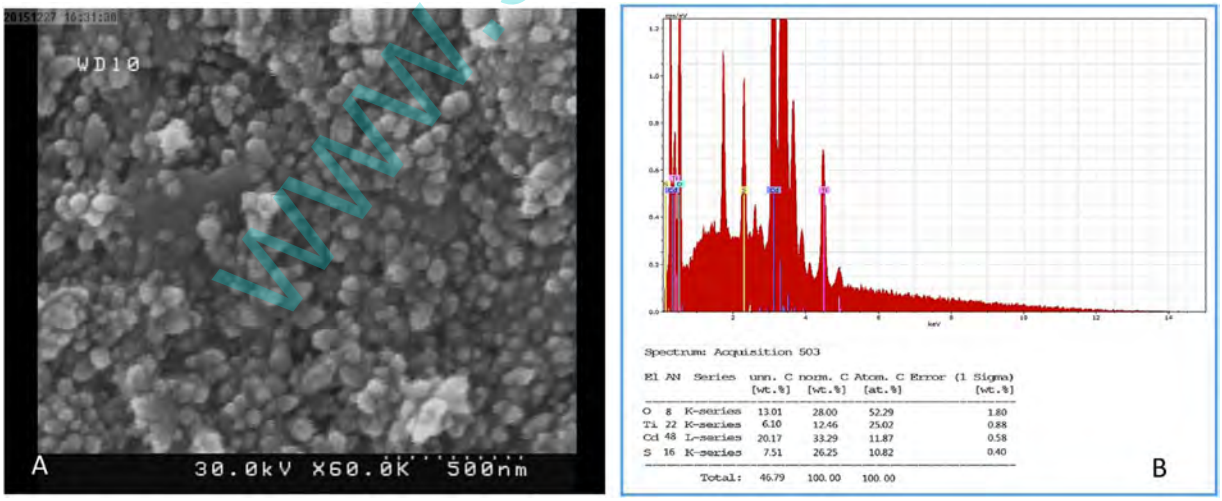

Fig. 7. (A) SEM images of the samples FTO/TiO_2/CdS thin film obtained from of TiO_2 nanorods prepared by the CBD technique with CdS nanoparticles by successive ionic layer adsorption and reaction (SILAR). (B) EDX spectrum of FTO/TiO_2 NRs/CdS NPs (CBD/SILAR) core-shell film.

total coverage of the substrate with TiO_2 conical rods is preferable on the substrate surface. The whole surface was composed of conical NR structures, which are composed of NRs and NR bundles. The length of an NR was in the range of approximately 120–210 nm, and the diameter was in the range of approximately 30–50 nm. These results are in a good agreement with other published results such as those by More et al. [30]. The intercrystalline barrier effect of TiO_2 decreased using NR shape instead of a porous shape of TiO_2 thin film. This characteristic might have contributed to decrease in the ohmic loss through the TiO_2 layer in dye-sensitized solar cells because of the easier

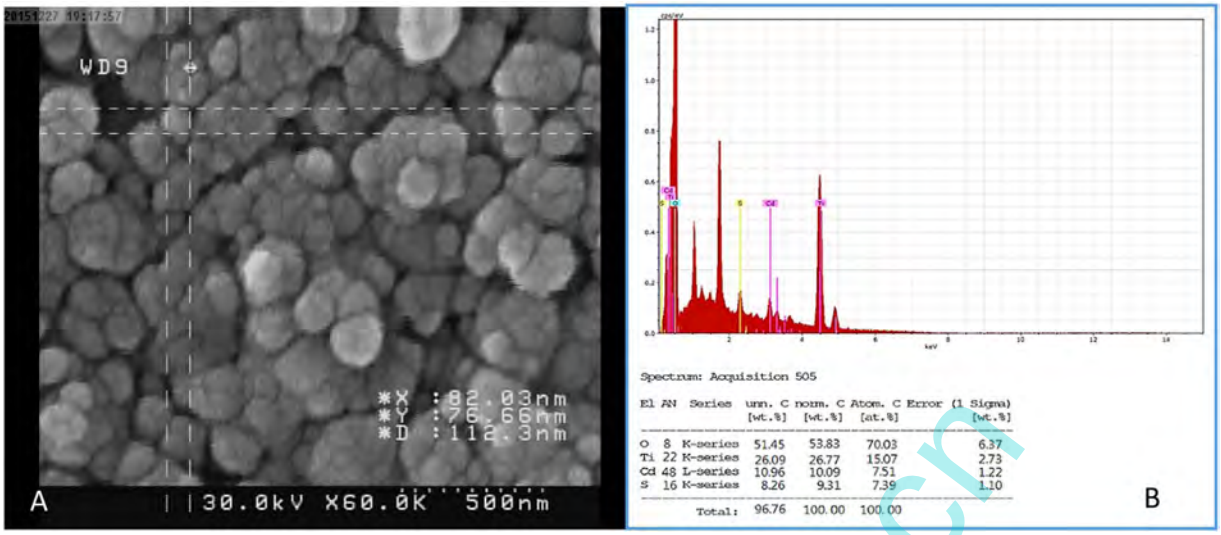

Fig. 8. (A) SEM images of the samples FTO/TiO_2/CdS thin film obtained from of TiO_2 nanograined prepared by the SILAR technique with CdS nanoparticles by successive ionic layer adsorption and reaction (SILAR). (B) EDX spectrum of FTO/TiO_2/CdS (SILAR/SILAR) core-shell film.

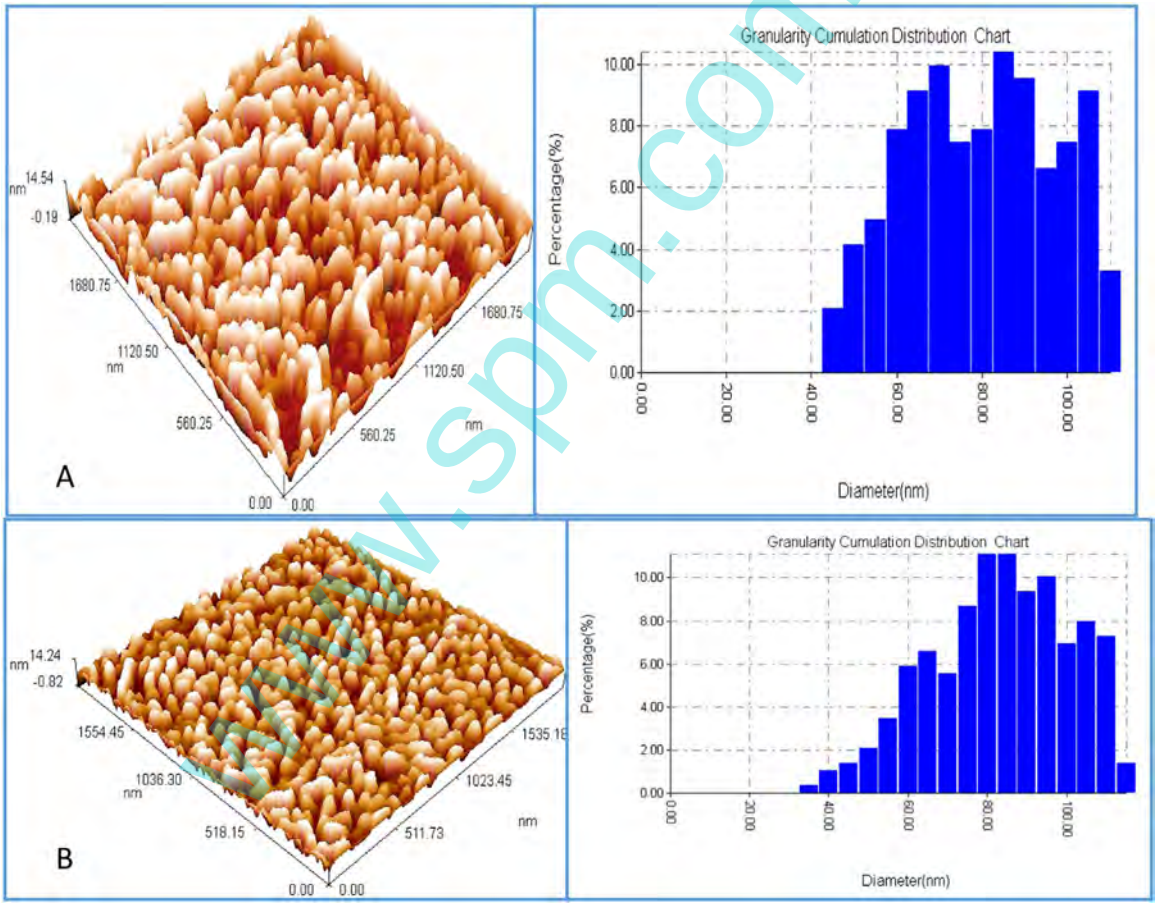

Fig. 9. Three dimension AFM images of (A) FTO/TiO_2 thin films deposited by CBD. (B) FTO/TiO_2 thin films deposited by SILAR.

electron transfer [30,31].

Fig. 6A and B shows the scanning electron micrographs of TiO_2 thin films deposited by SILAR for one and ten cycles on FTOCGS, respectively. Fig. 6A depicts that FTOCGS was completely covered with spherical nanograined TiO_2 particles. The average grain size increased from 43 nm for one cycle to 88 nm for ten cycles because the TiO_2 nanocrystallites aggregated and formed larger crystallites [23]. The grain size estimated using the scanning electron micrographs was much larger than that of XRD using Scherrer's equation, because the former detects formation of particles with different shapes and sizes. The scanning electron micrographs show grain agglomerates. These results are consistent with the results published by Deshmukh et al. [6]. Patil et al. [5] reported the formation of nanosized smooth grains with some pits and mesosized pores over the surface.

Fig. 7A depicts the scanning electron micrographs of the TiO_2 NRs synthesized by CBD with CdS NPs deposited by SILAR. This technique

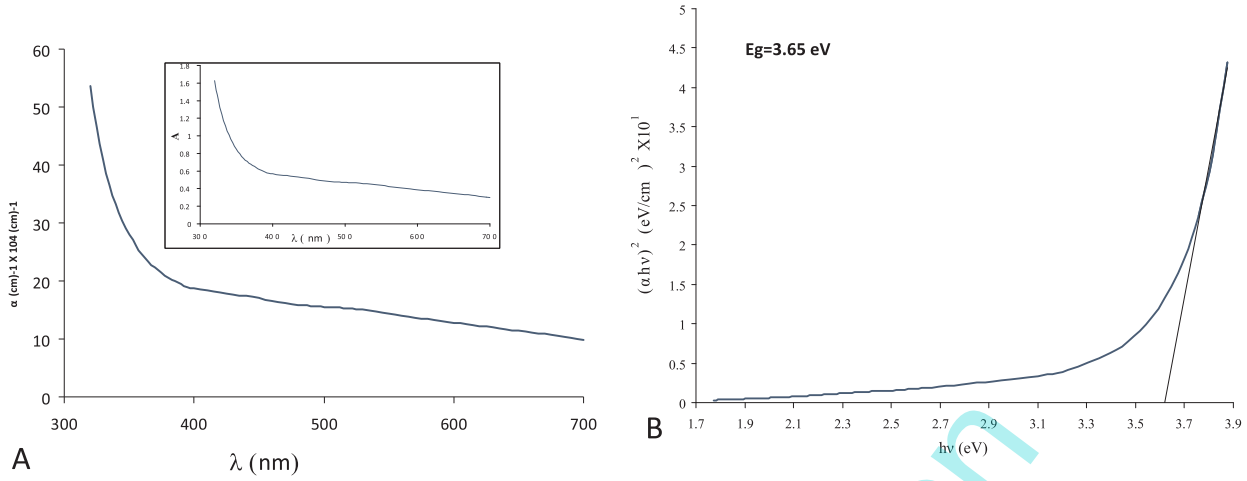

Fig. 10. (A) The absorption coefficient (α) versus wavelength of annealed TiO_2 thin film deposited by CBD. Inset plots of spectral absorption of annealed TiO_2 thin film. (B) plots of $(\alpha h\upsilon)^2$ versus photon energy for TiO_2 thin films.

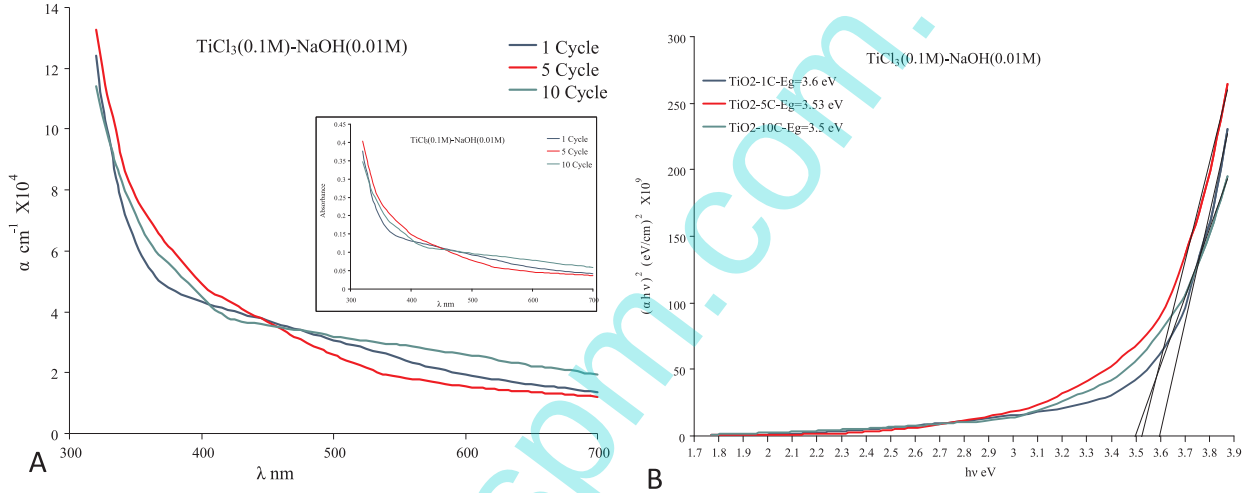

Fig. 11. (A) Absorption Coefficient (α) as a function of wavelength of TiO_2 thin film for different cycles deposited by SILAR. Inset plots of spectral absorption of TiO_2 thin film for different cycles. (B) Plots of $(\alpha h\upsilon)^2$ as a function of photon energy for TiO_2 thin films for different cycles.

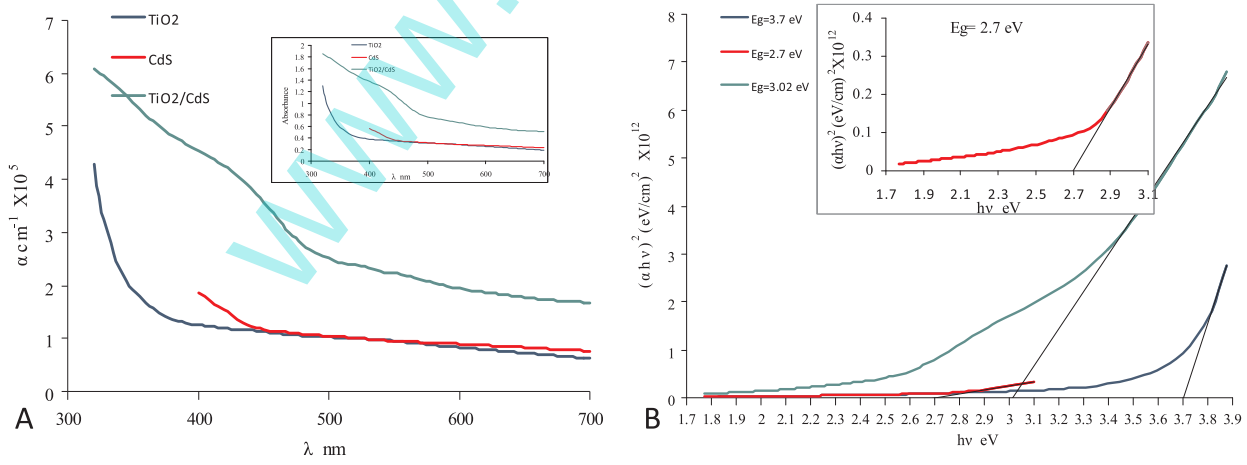

Fig. 12. (A) The absorption coefficient (α) versus wavelength of TiO_2 deposited by CBD, CdS deposited by SILAR, and TiO_2/CdS thin films. Inset plots of spectral absorption of thin films. (B) plots of $(\alpha h\upsilon)^2$ versus photon energy for TiO_2 thin films, CdS, and TiO_2/CdS thin films. Inset plots of$(\alpha h\upsilon)^2$ versus photon energy for CdS.

actively deposited CdS nanocrystallites on TiO_2 NRs. The scanning electron micrograph shows that after the deposition of CdS NPs, the entire surface of the NRs TiO_2 became uniformly covered with dense CdS spherical grains. The average diameter of the nanospherical grains was approximately 25 nm.

EDX analysis of the FTO/TiO_2/CdS NRs (Fig. 7B) indicated that the chemical structure of the core–shell NRs consisted of O (28), Ti (12.46), Cd (33.26), and S (26.25). These data confirm that the demonstrating the successful coating of CdS nanoparticles on the surface of TiO_2 nanorods [21,32].

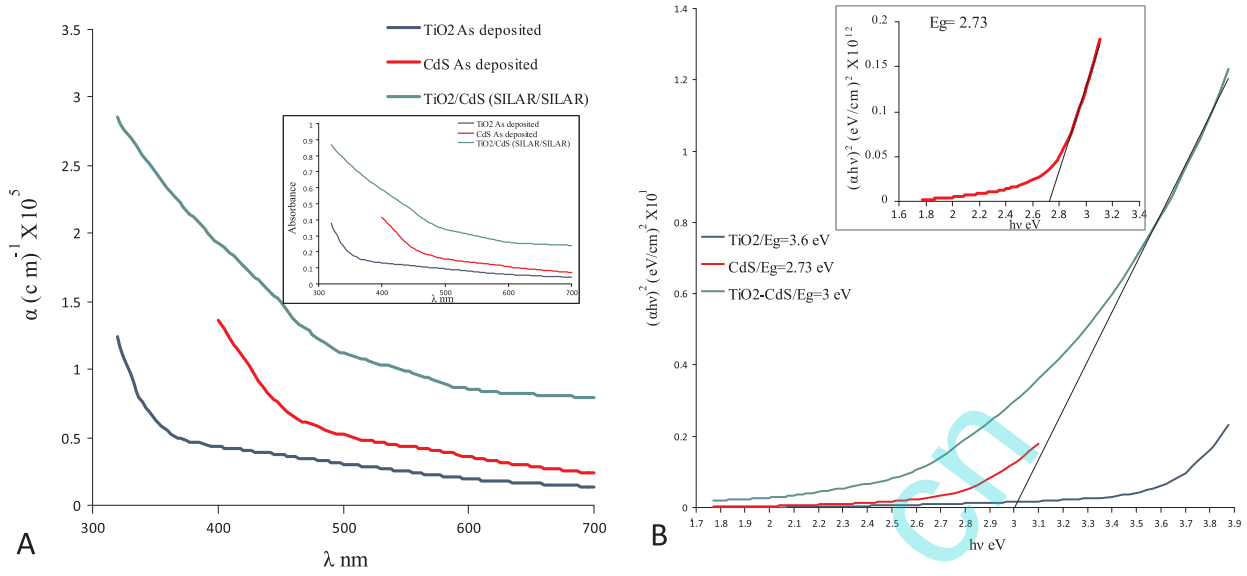

Fig. 13. (A) The absorption coefficient (α) versus wavelength of TiO_2 deposited by SILAR, CdS deposited by SILAR, and TiO_2/CdS thin films. Inset plots of spectral absorption of thin films. (B) plots of $(\alpha\ h\upsilon)^2$ versus photon energy for TiO_2 thin Films, CdS, and TiO_2/CdS thin films. Inset plots of $(\alpha\ h\upsilon)^2$ versus photon energy for CdS.

Table 2
Energy band values for TiO_2, CdS, and TiO_2/CdS deposited by chemical methods.

Chemical methods	Eg (eV) for TiO_2	Eg (eV) for CdS	Eg (eV) for TiO_2/CdS
CBD	3.7	2.7	3.02
SILAR	3.6	2.7	3

Fig. 8 displays the scanning electron micrograph of TiO_2 nanograin synthesized by SILAR for one cycle with CdS NPs deposited by SILAR. The scanning electron micrograph shows clusters of cauliflower-like grains with various sizes in the films with average grain size of approximately < 80 nm and contains blanks. Fig. 8 shows large CdS crystallites consisting of several nanocrystallites deposited on the TiO_2 nanograins. Deshmukh et al. [6] and Mane et al. [33] reported similar nanograined morphology over FTO substrate.

EDX quantitative analysis of the top surface of FTO/TiO_2 NRs/CdS indicated an approximately 2:1 stoichiometric ratio of O to Ti (O = 53.83%; Ti = 26.77%) and 1:1 stoichiometric ratio of Cd to S (Cd = 10.09%; S = 9.31%). This result is expected for the TiO_2 and CdS compounds (Fig. 8B), confirming the formation of a CdS layer on TiO_2 film. Cao et al. [21] and Li et al. [34] used the EDX to analysis the chemical composition of the CdS over TiO_2 nanrods and ZnO over TiO_2 nanotube, respectively.

Fig. 9A shows the three-dimensional (3D) AFM images of TiO_2 thin film deposited by CBD. These micrographs show that the thin films of TiO_2 had homogeneous surfaces with cylindrical shaped (rods) particles with semi-regular size and uniform distribution with empty size between rods. The average grain size for this sample was 77 nm. The average roughness (AR) was approximately 1.68 nm, and root mean square (RMS) was 2.25 nm. Fig. 9B shows the typical 3D AFM image of TiO_2 thin films deposited by SILAR. The surface of the film was very compact. The film constituted spherical shaped particles packed together and had regular size distribution. AFM results show that the average grain size of the films was 80 nm. The AR and RMS were approximately 0.725 nm and 0.847 nm, respectively.

3.3. Optical study

Variation in the absorbance with wavelength was determined to investigate the optical characteristics of the annealed TiO_2 films as shown in the inset in Fig. 10A. These spectra revealed that TiO_2 films had low absorbance in the visible region, which was attributed to the scattering of light caused by blanks in the nanorods [35]. The recorded absorption coefficient of the TiO_2 films with thickness of 145 nm (all the films have the same thickness) is depicted in Fig. 10A. The films had large absorption coefficient at short wavelength, and then the coefficient decreased to a constant value at 340 nm and longer. The films became transparent at long wavelength (above 340 nm). The value of

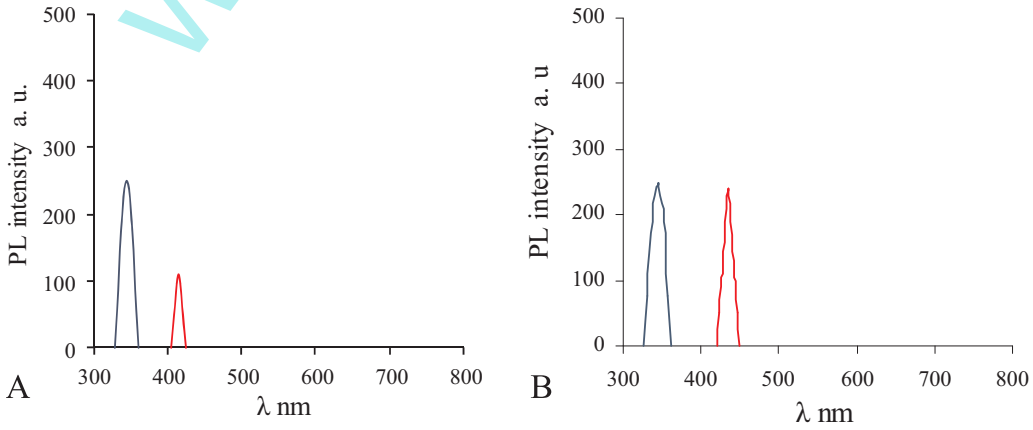

Fig. 14. Photoluminescence spectra of the (A) TiO_2 deposited by CBD, and (B) TiO_2 deposited by SILAR.

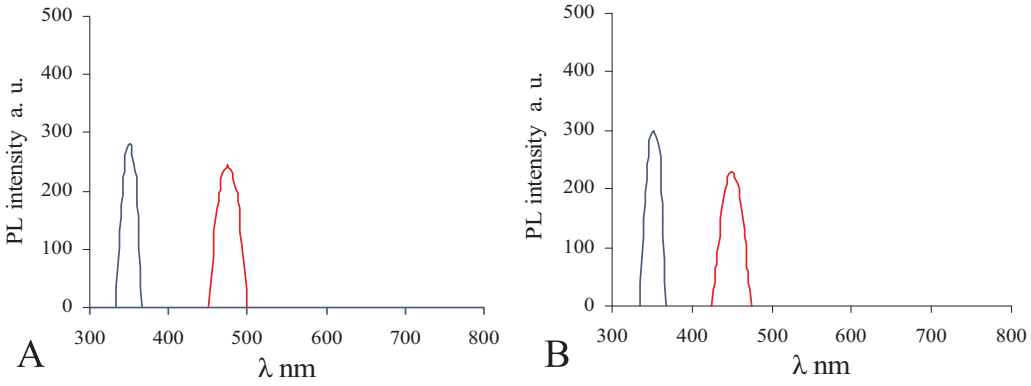

Fig. 15. Photoluminescence spectra of the (A) TiO_2/CdS NPs (CBD/SILAR), and (B) TiO_2/CdS NPs (SILAR/SILAR for 1 cycle) films.

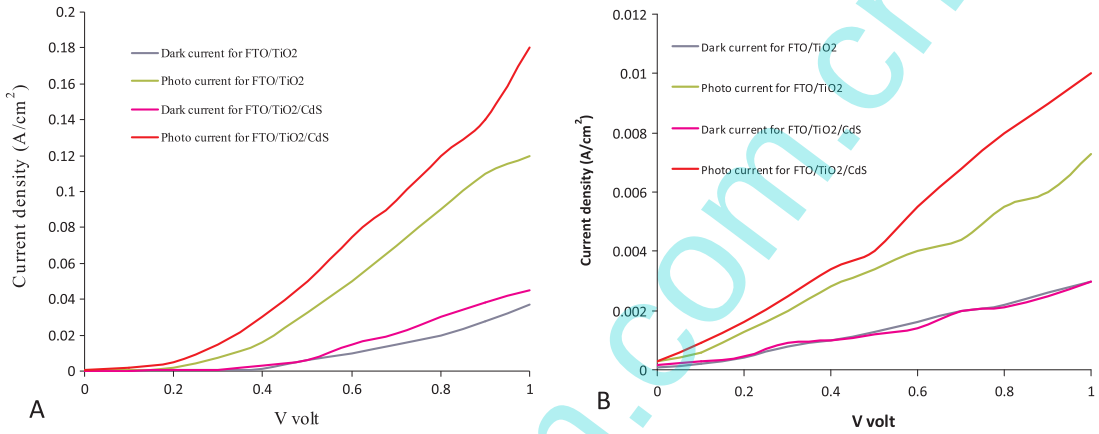

Fig. 16. Photocurrent versus potential voltage for thin film electrodes of TiO_2 and TiO_2/CdS. (A) TiO_2 deposited by CBD. (B) TiO_2 deposited by SILAR under the visible-light illumination (100 mW/cm^2).

the energy gap was evaluated by extrapolating the straight line of $(\alpha h\upsilon)^2$ plotted as function of the photon energy of the samples (Fig. 10B). The linear relation between $(\alpha h\upsilon)^2$ and $h\upsilon$ denotes a direct band gap, which was found to be 3.65 eV. This value was higher than that of bulk anatase TiO_2 (3.2 eV), because the optical band gap energy is dependent on grain size (quantum size effect) [36,37].

Data from the transmission spectrum were used to calculate the absorption coefficient. The absorption spectra of TiO_2 samples were recorded at several numbers of cycles as shown in Fig. 11. Fig. 11A evidently displays that the absorption coefficients of the films were higher in the short-wavelength range (320–400 nm). Depending on the film structure, the absorption coefficients decreased at different rates to constant values at long wavelengths where the samples become transparent. The optical properties of TiO_2 films were investigated from the variation in optical absorbance with wavelength as shown in the inset of Fig. 11A.

Fig. 11B displays the effect of number of cycles on the energy gap. The samples show a relative decrease in energy gap with increasing number of cycles. The decrease in the energy gap in the samples is due to the grain size growth as identified by XRD.

The results of CdS preparation were examined by the absorption measurement in the range of 320–700 nm. Fig. 12A displays the optical absorption spectra of FTO/TiO_2 deposited by CBD, FTO/CdS deposited by SILAR, and FTO/TiO_2/CdS thin films at room temperature without considering the losses caused by transmission and reflection. The TiO_2 films show an absorption in the UV region (at < 335 nm), and its low absorption in the visible region could have resulted from the scattering of the light by the blanks in the NRs. By contrast, the absorption edge of FTO/TiO_2/CdS thin film was highly extended to the visible region, because the deposition of CdS NPs upon TiO_2 NRs showed strong absorption in a wide range. The CdS deposited on FTO/TiO_2 substrate exhibited band edge absorption at 410 nm, while the CdS deposited on FTOCGS have characteristic absorption edge at 500 nm (as shown in the inset of Fig. 12B). Blue-shift was observed in the CdS deposited on TiO_2 substrate versus that deposited on the FTOCGS, which indicates evident size quantization effect of the NPs [6]. Similar optical characteristics of CdS over TiO_2 NR were reported by Xie et al. [23], but they deposited TiO_2 by oxidizing Ti NRAs. The absorption ability in the visible light of the CdS deposited on NRs TiO_2 increased, which may suggest an increasing photocatalytic activity for core–shell NRs TiO_2/CdS in the visible light [21].

Fig. 13A shows the optical absorption spectra for FTO/TiO_2 deposited by SILAR, FTO/CdS deposited by SILAR, and FTO/TiO_2/CdS core–shell system. FTO/TiO_2 had absorbance in the UV region with a wavelength below 340 nm because of a large energy band gap for TiO_2NRs. CdS exhibited absorbance in the visible region with a wavelength below approximately 500 nm. The FTO/TiO_2/CdS core–-shell system shows enhanced absorbance in the visible light region. By contrast, TiO_2 NR thin films deposited by CBD exhibited higher absorption in the visible region than nanograined TiO_2 thin films deposited by SILAR. This phenomenon is due to the high surface area of TiO_2 NRAs as shown by the scanning electron micrograph, leading to high absorption ability in the visible light of the CdS deposited on TiO_2 NR (inset of Fig. 13A compared with inset of Fig. 12A). The energy band values for thin films deposited by chemical methods are provided in Table 2.

Fig. 14 shows the typical room-temperature PL spectra of the TiO_2 thin films. The emission of TiO_2 deposited by CBD (Fig. 14A) is generally classified into two categories. One category is the UV emission of the near band edge (NBE) in the UV region at 338 nm (3.67 eV). This characteristic is related to the direct band gap transition and/or free-exciton recombination. The other region is the deep-level

emission in the visible range at 420 nm. This region originated from defects, such as oxygen vacancies or TiO_2 interstitials. Fig. 14B shows TiO_2 films deposited by SILAR. An evident shift in the peak located in the UV region was found to be 344 nm (3.6 eV), instead of 338 nm (3.67 eV).

The PL peak positions of the TiO_2/CdS (TiO_2 deposited by CBD) were found at 350 nm and 475 nm as shown in Fig. 15A. These peaks could have been caused by the NBE emission of TiO_2 and the quantum size effect of CdS [20,21], respectively, or by the defect-assisted recombination in CdS. The broad PL features may have been caused by the quantum size effect in the core-shell thin film [20]. Fig. 15B shows the PL spectra of TiO_2/CdS (TiO_2 deposited by SILAR). A broad peak was located in the UV region at 352 nm, which represents the NBE of TiO_2. Another peak centered at 425 nm was broader and with weaker intensity, because the SILAR method produces very fine TiO_2 layer for one cycle.

3.4. *I–V characteristics*

The *I–V* curves of FTO/TiO_2 and FTO/TiO_2/CdS electrode tested in the dark and under illumination are shown in Fig. 16. The dark current densities of two samples were found to be very low. In the dark, the nonlinear nature of *I–V* curves predict that the FTO/TiO_2 and FTO/TiO_2/CdS make rectification contact with the electrolyte [5,6]. The photocurrent increased from 0.12 A/cm^2 for TiO_2 deposited by CBD to 0.18 A/cm^2 for TiO_2/CdS system, indicating an approximately 1.5-fold increase, and from 7.3 mA/cm^2 for TiO_2 deposited by SILAR to 10 mA/cm^2 for TiO_2/CdS system, exhibiting an approximately 1.37-fold increase. The enhanced PEC performance of TiO_2/CdS system may be attributed to the increasing absorption ability in the visible light of the CdS deposited on TiO_2 as shown from the optical study. In addition to the aforementioned factors, several studies have attributed this phenomenon to the following factors: (1) reduction in the recombination rate of electron–hole; (2) charge in separation improvement; (3) enhanced interfacial charge transfer efficiency to adsorbed substrate, and (4) improved lifetime of the charge carrier [21,23,38]. TiO_2 NR thin films deposited by CBD for TiO_2/CdS system exhibited higher photo current than nanograined TiO_2 thin films deposited by SILAR for TiO_2/CdS system because of the high contact area between CdS QDs and electrolyte [22]. This characteristic was due to the uniformly covered surface of the TiO_2 NRs with dense CdS spherical grains, resulting in large surface area [39] more suitable for PEC application [33]. Moreover, the barrier effect of intercrystalline TiO_2 was reduced using long NRs instead of nanograined TiO_2 thin film, resulting in easier electron transfer and reduced ohmic loss through the TiO_2 layer [30,40].

4. Conclusion

Low-cost, simple, and efficient methods were used to fabricate TiO_2/CdS core–shell system. Structural, surface morphological, and optical characterizations of FTO/TiO_2, FTO/CdS, and FTO/TiO_2/CdS core– shell system were performed. Optical measurements showed that the band gaps were 3.7 eV and 3.6 eV for TiO_2 thin films deposited by CBD and SILAR, respectively. The absorption ability in the visible light of the CdS deposited on NRs TiO_2 increased. Scanning electron micrographs also show the polycrystalline nature of films with NR structure for TiO_2 deposited by CBD and nanograined structure for TiO_2 deposited by SILAR. This study also reveals that CBD is a simple and viable method for producing TiO_2 thin films with high surface area. The PEC performance of the TiO_2 NR thin films deposited by CBD was enhanced compared with that of the nanograined TiO_2 thin films deposited by SILAR.

References

[1] M. Mahalakshmi, J. Nano Sci. Nano Technol. 2 (2014) 424–427.
[2] H.U. Igwe, O.E. Ekpe, E.I. Ugwu, Res. J. Appl. Sci. Eng. Technol. 2 (5) (2010) 447–451.
[3] M. Lezner, E. Grabowska, A. Zaleska, Physicochem. Probl. Miner. Process. 48 (1) (2012) 193–200.
[4] H.A. Shukur, M. Sato, I. Nakamura, I. Takano, Adv. Mater. Sci. Eng. 923769 (2012) 1–7.
[5] U.M. Patil, K.V. Gurav, Oh-Shim Joo, C.D. Lokhande, J. Alloy. Compd. 478 (2009) 711–715.
[6] P.R. Deshmukh, U.M. Patil, K.V. Gurav, S.B. Kulkarni, C.D. Lokhande, Bull. Mater. Sci. 35 (2012) 1181–1186.
[7] H. Feng Lu, Feng Li, G. Liu, Zhi-Gang Chen, Da-Wei Wang, Hai-Tao Fang, Gao Qing Lu, Z. Hua Jiang, Hui-Ming Cheng, Nanotechnology 19 (405504) (2008) 7.
[8] P.R. Ohodnicki, J. Congjun Wang, S. Natesakhawat, J.P. Baltrus, T.D. Brown, J. Appl. Phys. 111 (2012) (064320-1-11).
[9] Tae-Sik Kang, A.P. Smith, B.E. Taylor, M.F. Durstock, Nano Lett. 9 (2009) 601–606.
[10] S.M.H. AL-Jawad, A.K. Elttayf, A.S. Saber, Surf. Rev. Lett. 24 (7) (2017) 1750104 (13 pages).
[11] A. López, D. Acosta, A.I. Martínez, J. Santiago, Powder Technol. 202 (2010) 111–117.
[12] I. Oja Acik, A. Junolainen, V. Mikli, M. Danilson, M. Krunks, Appl. Surf. Sci. 256 (2009) 1391–1394.
[13] Ali M. Al-Zuhery, Selma M. Al-Jawad, Ali K. Al-Mousoi, Optik 130 (2017) 666–672.
[14] D.R. Acosta, A. Martı´nez, C.R. Magan˜a, J.M. Ortega, Thin Solid Films 490 (2005) 112–117.
[15] N.S. Begum, H.M. Farveez Ahmed, Bull. Mater. Sci. 31 (2008) 43–48.
[16] L. Xiangqing, Y. Cheng, L. Liu, Jin Mu, Colloids Surf. A: Physicochem. Eng. Asp. 353 (2010) 226–231.
[17] E. Pentia, L. Pintilie, I. Matei, T. Botila, E. Ozbay, J. Optoelectron. Adv. Mater. 3 (2) (2001) 525–530.
[18] H. Zhang, X. Ma, J. Xu, J. Niu, J. Sha, D. Yang, J. Cryst. Growth 246 (2002) 108–112.
[19] R.C. Rodriguez, A.I. Oliva, V. Sosa, F.C. Briones, J.L. Pena, Appl. Surf. Sci. 161 (2000) 340–346.
[20] K.K. Challa, S.K. Goswami, E. Oh, E. Tae Kim, Appl. Phys. Lett. 99 (2011) 1–3.
[21] C. Cao, C. Hu, W. Shen, S. Wang, Y. Tian, X. Wang, J. Alloy. Compd. 523 (2012) 139–145.
[22] Y. Hu, B. Wang, J. Zhang, T. Wang, R. Liu, J. Zhang, X. Wang, H. Wang, Nanoscale Res. Lett. 8 (222) (2013) 1–5.
[23] Z. Xie, X. Liu, W. Wang, C. Liu, Z. Li, Z. Zhang, Sci. Technol. Adv. Mater. 15 (2014) 1–10.
[24] Y. Li, L. Zhang, W. Wu, P. Dai, X. Yu, M. Wu, G. Li, Nanoscale Res. Lett. 9 (2014) 1–6.
[25] L. Yu, D. Wang, Daiqi Ye, Sep. Purif. Technol. 156 (2015) 708–714.
[26] P. Sun, X. Zhang, C. Wang, Y. Wei, L. Wang, Y. Liu, J. Mater. Chem. A 1 (2013) 3309–3314.
[27] B.D. Cullity, S.R. S tock, Elements of X–Ray Diffraction, 3rd ed., Prentice-Hall, United States of America, 2001.
[28] S.M.H. AL-Jawad, A.K. Elttayf, A.S. Saber, Surf. Rev. Lett. 24 (7) (2017) 1750110 (pp. 12).
[29] S. Chen, M. Paulose, C. Ruan, G.K. Mor, O.K. Varghese, D. Kouzoudis, C.A. Grimes, J. Photochem. Photobiol. A: Chem. (2006) 177–184.
[30] A.M. More, T.P. Gujar, J.L. Gunjakar, C.D. Lokhande, Joo Oh-Shim, Appl. Surf. Sci. 255 (2008) 2682–2687.
[31] A.K. Singh, S.B. Patil, U.T. Nakate, K.V. Gurav, J. Chem. 2013 (2013) 1–8.
[32] A. Trenczek-Zajac, A. Kusior, A. Lacz, M. Radecka, K. Zakrzewska, Mater. Res. Bull. 60 (2014) 28–37.
[33] R.S. Mane, Y.H. Hwang, C.D. Lokhande, S.D. Sartale, S.H. Han, Appl. Surf. Sci. 246 (2005) 271–278.
[34] R. Li, Z. Xie, H. Lu, D. Wei Zhang, A. Yu, Int. J. Electrochem. Sci. 8 (2013) 11118–11124.
[35] G. Li, L. Wu, F. Li, P. Xu, D. Zhang, H. Li, Nanoscale 5 (2013) 2118–2125.
[36] R.C. Rodriguez, A.I. Oliva, V. Sosa, F.C. Briones, J.L. Pena, Appl. Surf. Sci. 161 (2000) 340–346.
[37] R.A. Ismail, S.M.H. Al-Jawad, N. Hussein, Appl. Phys. A Mater. Sci. Process. 117 (2014) 1977–1984.
[38] Y. Bessekhouad, D. Robert, J.-V. Weber, J. Photochem. Photobiol. A: Chem. 163 (2004) 569–572.
[39] Jong-Hyun Yoon, Song-Rim Jang, R. Vittal, Jiwon Lee, Kang-Jin Kim, J. Photochem. Photobiol. A: Chem. 180 (2006) 184–188.
[40] J. Jiu, S. Isoda, F. Wang, M. Adachi, J. Phys. Chem. B 110 (2006) 2087–2093.